Integrating Enrichment, Reduction and Oxidation Sites in One System for Artificial Photosynthetic diluted CO_2 Reduction

Yan Yang[a,c,†], Hong-Yu Zhang[a,c,†], Ya Wang[a,†], Lu-Hua Shao[a], Liang Fang[a], Hong Dong[a], Meng Lu[b], Long-Zhang Dong[b], Ya-Qian Lan[b] and Feng-Ming Zhang[a,]*

[†]These authors contributed equally to this work.

[*]Corresponding Author.

Y. Yang, H.-Y. Zhang, Y. Wang, L.-H. Shao, L. Fang, H. Dong, Prof. F.-M. Zhang

[a] Heilongjiang Provincial Key Laboratory of CO_2 Resource Utilization and Energy Catalytic Materials, School of Material Science and Chemical Engineering, Harbin University of Science and Technology, No. 52, Xuefu Road, Harbin, 150040, P. R. China.

E-mill: zhangfm80@163.com.

This article has been accepted for publication and undergone full peer review but has not been through the copyediting, typesetting, pagination and proofreading process, which may lead to differences between this version and the Version of Record. Please cite this article as doi: 10.1002/adma.202304170.

Dr. M. Lu, L.-Z. Dong, Prof. Y.-Q. Lan

[b] School of Chemistry, South China Normal University, Guangzhou, 510006, P. R. China.

Y. Yang, H.-Y. Zhang

[c] School of Chemistry and Chemical Engineering, Harbin Institute of Technology, Harbin,150001, P. R. China.

Keywords: Three-in-one photocatalysts, Covalent organic frameworks, Ionic liquids, Diluted CO_2 reduction, Natural sunlight driven.

Abstract: Artificial photosynthetic diluted CO_2 reduction directly driven by natural sunlight is a challenging but promising way to realize carbon-resources recycling utilization. Herein, a three-in-one photocatalytic system of CO_2 enrichment, CO_2 reduction and H_2O oxidation sites was designed for diluted CO_2 reduction. A Zn-Salen-based covalent organic framework

(Zn-S-COF) with oxidation and reductive sites was synthesized, then ionic liquids (ILs) were loaded into the pores. As a result, [Emim]BF_4@Zn-S-COF shows a visible-light-driven CO_2-to-CO conversion rate of 105.88 μmol·g^{-1}·h^{-1} under diluted CO_2 (15%) atmosphere, even superior than most photocatalysts in high concentrations CO_2. Moreover, natural sunlight driven diluted CO_2 reduction rate also reached 126.51 μmol·g^{-1} in 5 h. Further experiments and theoretical calculations reveal that the triazine ring in Zn-S-COF promotes the activity of H_2O oxidation and CO_2 reduction sites, and the loaded ILs provide an enriched CO_2 atmosphere, realizing the efficient photocatalytic activity in diluted CO_2 reduction.

1. Introduction

Mimicking natural photosynthesis to direct capture and in-situ reduction of diluted CO_2 into fuels or high value-added chemicals is an intriguing strategy for the recycle and utilization of carbon resources.[1] Solar-energy-driven CO_2 reduction meets the requirement of recycle and utilization of carbon resources by green way owning to its inexhaustible and clean merits of sunlight. Over the past decades, various semiconductors based artificial photocatalysts have been developed to achieve efficiently converting from CO_2 to the aimed products, with high activity and selectivity.[2] Nevertheless, most of these investigations and activity assessments

of photocatalysts were based on high-concentration CO_2 atmosphere, and limited attempts of diluted CO_2 photocatalytic reduction often give relatively low catalytic activity. In fact, the producing process of concentrated CO_2 is of high energy consumption in industrial production. Considering that the concentration of CO_2 in the exhaust gases is relatively low (10~15%), the development of robust catalysts that can efficiently convert diluted CO_2 to desirable products is a critical step towards future practical CO_2 resource utilization.[3] One of the primary reasons leading to the low activity of photocatalysts in diluted CO_2 atmosphere is that the capturing process of CO_2 molecules in diluted atmosphere prolongs the overall reaction time.[4]

Crystalline and porous materials, such as metal-organic frameworks (MOFs) and covalent organic frameworks (COFs), are emerging types of photocatalysts with high surface area, tunable pore size and band positions, which possess intrinsic merits in absorbing gas substrate in catalytic reaction due to their structural porosity.[5] Different from MOFs, two dimensional (2D) COFs are assembled by covalent connection of pure organic building blocks, which generally possess large conjugated system, layered structure and prominent visible-light-harvesting ability as photocatalysts.[6] Metal-covalent organic frameworks (M-COFs), formed by anchoring metal ions onto the backbone of COFs, combine the

photocatalytic advantages of MOFs with abundant metal centers and the features of COFs photocatalysts, which are considered as a new type of promising catalysts for CO_2 photoreduction.[7] Moreover, this type materials inherit the porous character of its parent COFs/MOFs, which offer great opportunity for further functionality to endow the resultant materials with special or enhanced property.[8] Previously, we and other groups employed the structural advantages of M-COFs to construct a series of two-in-one photocatalytic systems by coupling photocatalytic CO_2 reduction and H_2O oxidation centers for artificial photosynthesis CO_2 reduction.[9] Although the these materials effectively drive photocatalytic overall reductive and oxidative reactions with pure CO_2 as source, their photocatalytic diluted CO_2 reduction activities are relatively low primarily due to the absence of effective CO_2 enriching component.

Ionic liquids (ILs) are a type of famous candidates for CO_2 absorption and selective capture of diluted CO_2 under atmospheric pressure.[10] The unique properties of ILs, including negligible vapor pressure, high thermal stability, and virtually unlimited tunability, enable their practical application in CO_2 capture and separation field.[11] The interaction modes of CO_2 and ILs can be versatile, including physical absorption, weak interaction and chemical interaction.[12] Moreover, ILs acting as functional species have been loaded into porous MOFs

to substantially enhance their CO_2 absorption ability.[13] Thus, we reasoned that loading ILs into porous M-COFs may not only enhance selective absorption towards diluted CO_2, but also create a high-concentration CO_2 atmosphere for host photocatalysts benefiting photocatalytic diluted CO_2 reduction reaction.

With the above in mind, for the first time, we constructed a three-in-one artificial photosynthetic system with M-COF and ILs, which combine the CO_2 reduction, H_2O oxidation and CO_2 enrichment centers together for efficiently reducing diluted CO_2 (**Figure 1**). A new Zn-S-COF with oxidation and reductive sites was designed and synthesized, then ILs acting as CO_2 enrichment component were introduced into the pores of Zn-S-COFs. As confirmed, the [Emim]BF_4@Zn-S-COF shows a CO_2-to-CO conversion rate of 267.95 $\mu mol \cdot g^{-1} \cdot h^{-1}$, which is 17 times higher than that of the pristine Zn-S-COF. Moreover, under diluted CO_2 (15%) atmosphere, the three-in-one photocatalyst shows a high photocatalytic CO_2-to-CO conversion activity of 105.88 $\mu mol \cdot g^{-1} \cdot h^{-1}$ and a surprising CO evolution amount of 126.51 $\mu mol \cdot g^{-1}$ in 5 h under natural sunlight. The stable coordination environment of Zn-Salen centers in the reaction process was validated by X-ray absorption spectra (XAS). Further experiments and DFT calculations reveal that the loaded ILs provide an enriched CO_2 atmosphere while the triazine ring in Zn-S-COF promotes the activity of H_2O oxidation and

CO_2 reduction sites. This work provides a new design strategy for the construction of artificial photosynthetic catalysts for directly reducing diluted CO_2.

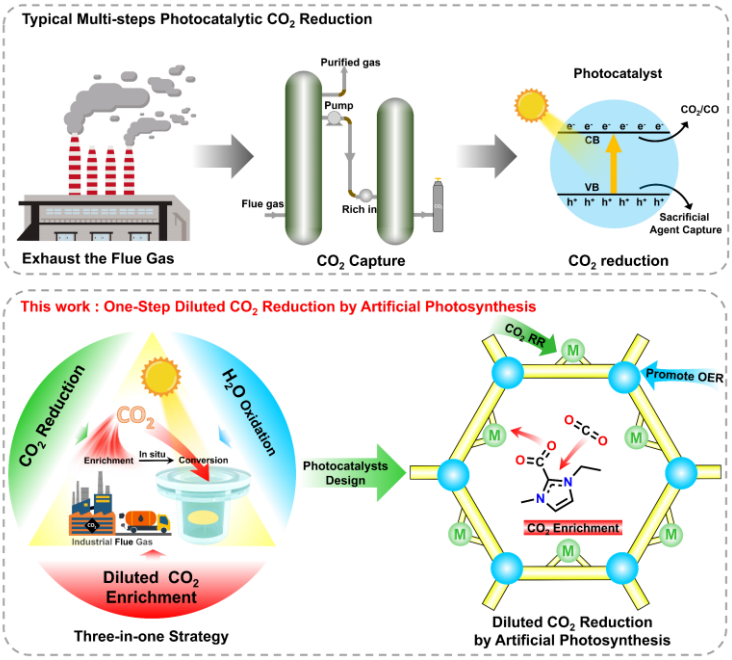

Figure 1. Schematic diagram of the three-in-one design strategy of one-step diluted CO_2 reduction by artificial photosynthesis.

2. Results and Discussion

As shown in **Figure 2**a, Zn-S-COF was synthesized by acid-catalyzed Schiff base reaction of (1R,2R)-(-)-1,2-diaminocyclohexane and 1,3,5-triazine-2,4,6-tris(4´-hydroxy-5´-formylphenyl)benzene by in-situ adding

$Zn(ClO_4)_2 \cdot 6H_2O$ in mesitylene/ethanol =1:1 (V:V) solution at 120 °C for 3 days, giving yellow solid with the yield of ~86% (Figure S1). The introduction of Zn^{2+} plays a key role for the formation of crystalline Zn-S-COF due to the formed planar coordinational configuration of Zn-Salen unit. In the Fourier-transform infrared (FT-IR) spectra, the stretching vibration bands of C=O around 1658 cm^{-1} disappeared in Zn-S-COF, indicating the thorough consumption of aldehyde monomers. Meanwhile, a strong characteristic peak at 1638 cm^{-1} from C=N bonds appeared for Zn-S-COF, suggesting the formation of polymeric structure (Figure S2).[14]

The crystalline nature of Zn-S-COF was determined by powder X-ray diffraction (PXRD) analysis. Two possible stacking modes of Zn-S-COF, overlapping stacking AA mode and the staggered stacking AB mode, were obtained by simulation, respectively (Figure 2b and Figure S3). The unit cell parameters were obtained after minimizing the geometric energy as $a = b = 28.80$ Å, $c = 3.5$ Å, $\alpha = \beta = 90°$, $\gamma = 120°$ (Table S2). As shown in Figure 2c, the experimentally measured PXRD diffraction peaks of Zn-S-COF match well with the AA stacking mode, the peaks at 3.54, 7.19, 9.46 and 25.37° corresponding to (100), (200), (210), (001) planes of *P*321 space group, respectively. The results of full profile pattern matching (Pawley) refinements show the unit cell parameters from refinement nearly equal to the

predictions with good agreement factors (R_p = 4.02% and R_{wp} = 4.43%). The PXRD peak appeared at 25.37° for Zn-S-COF correlate to the interlayer distance and the value of *d* spacing was calculated to be 3.51 Å. Moreover, the ^{13}C solid state nuclear magnetic resonance spectroscopy (^{13}C ssNMR) also presented the characteristic signals of C=N bonds at 167 ppm, further confirming the successful synthesis of Zn-S-COF (Figure S4).[15]

The porosity of the Zn-S-COFs was determined by N_2 adsorption-desorption analysis at 77 K with activated sample (Figure 2e). The calculated value of Brunauer-Emmett-Teller (BET) surface areas of Zn-S-COF is 595.41 $m^2 \cdot g^{-1}$. The total pore volume was estimated to be 0.963 $cm^3 \cdot g^{-1}$ for Zn-S-COF at P/P_0 = 0.99. The pore size of Zn-S-COF is approximately 1.98 nm, which is comparable to that from structure simulation (2.19 nm). The scanning electron microscope (SEM) images indicate the aggregation of Zn-S-COF particles (Figure S5). The elemental mapping images reveal that Zn is uniformly distributed within the whole material of Zn-S-COF. The transmission electron microscopy (TEM) images show that the Zn-S-COF exhibited layered morphology (Figure S6). Obvious lattice fringes with the lattice spacing of 3.47 Å could be observed in the high-resolution transmission electron microscopy (HR-TEM) image of Zn-S-COF (Figure 2d), in good agreement with interlayer distance from structure. The energy dispersive X-ray spectrum (EDS) diagrams illustrate that the content of Zn^{2+} in

Zn-S-COF is 7.19 wt% (Figure S7). Further, inductively coupled plasma-optical emission spectrometry (ICP-OES) measurement confirms that the average contents of Zn in Zn-S-COF is 7.20 wt%. The thermostability of Zn-S-COF was determined by thermogravimetric analysis (TGA) under air atmosphere, and the results confirm that Zn-S-COF is stable up to 280 °C (Figure S8). Moreover, the Zn-S-COF show high chemical stability as examined by PXRD for the samples after immersed in various water/organic solvents and acid/base solutions for 7 days, including dimethyl sulfoxide (DMSO), N,N-dimethylformamide (DMF), ethanol, boiling water, pH = 1~14 aqueous solutions, NaOH (5 M) and HCl (2 M) (Figure S9).

A typical ionic liquid with high CO_2 absorption ability, 1-ethyl-3-methylimidazole tetrafluoroborate ([Emim]BF_4) was selected and loaded into the pores of Zn-S-COF for preparing [Emim]BF_4@M-COFs materials. After introducing [Emim]BF_4, the diffraction peaks from the pores of Zn-S-COF decreased apparently, while the the intensity of the peaks can returned when removing the guest [Emim]BF_4 (Figure S10).[16] The N_2 adsorption-desorption isotherms shows that the BET surface areas of [Emim]BF_4(56.41 wt%)@Zn-S-COF was decreased to 291.75 $m^2 \cdot g^{-1}$, accompanied with significantly diminished pore size distribution, which support the successful loading of ILs in the pore of Zn-S-COF (Figure 2e). However,

the combination of COFs and ILs can substantially enhance CO_2 absorption as confirmed by CO_2 absorption measurements at 298 K for [Emim]BF_4@M-COFs with different ILs loading content (39.28, 56.41 and 65.99 wt%) (Figure S11). It was confirmed that the CO_2 absorption of [Emim]BF_4(56.41 wt%) @Zn-S-COF is superior than others with a CO_2 uptake amount of 1.75 mmol·g^{-1}, which is about 2.5 times higher than that of the pristine Zn-S-COF.

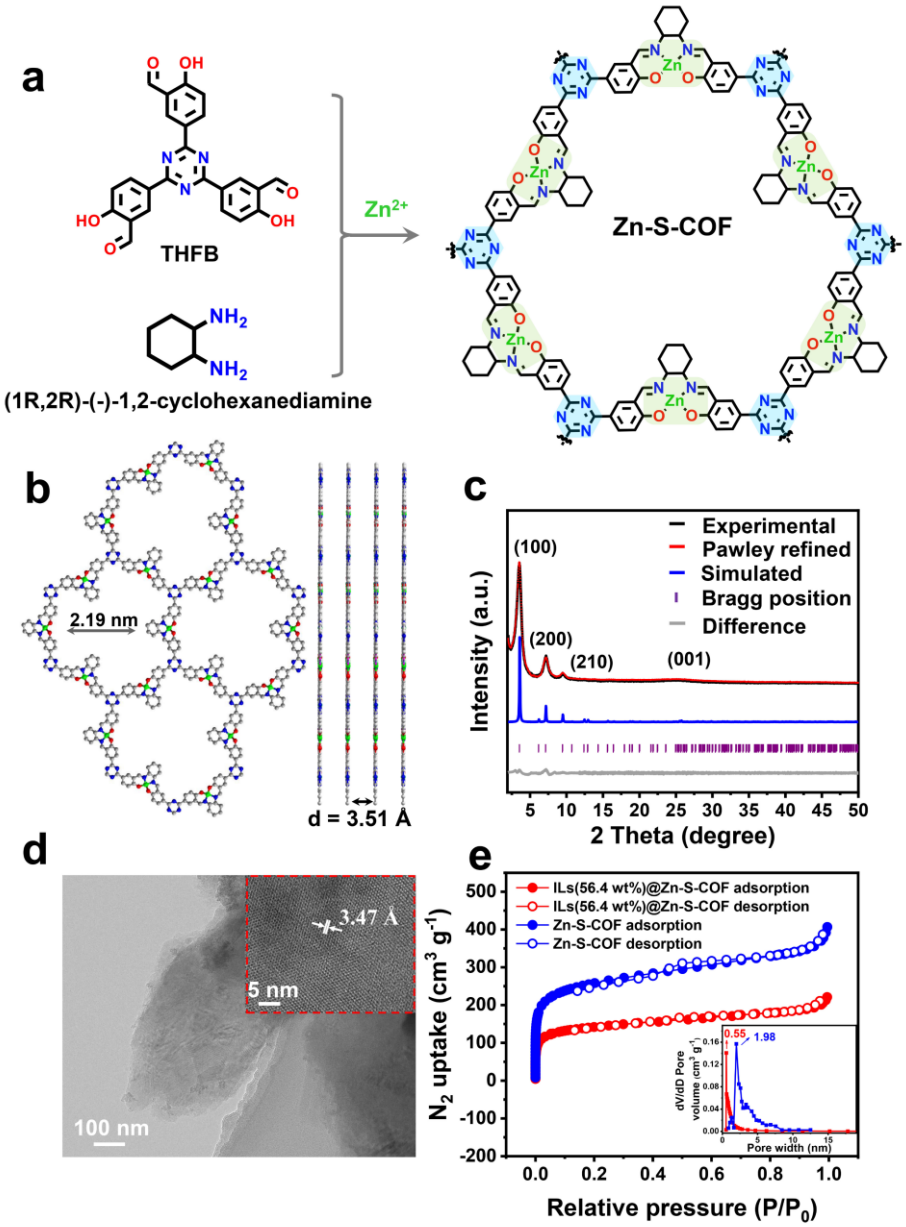

Figure 2. The preparation and characterization of Zn-S-COF. (a) Schematic diagram of Zn-S-COF synthesis. (b) Top and side views of Zn-S-COF with AA stacking mode. (c) PXRD

patterns of Zn-S-COF. (d) HR-TEM image and lattice fringes (insert) of Zn-S-COF. (e) N_2 adsorption-desorption isotherms (77 K) and pore size distribution profiles (insert).

For comparison, a Zn-CCOF with similar Salen segment but without triazine core was synthesized according reported method (**Figure 3**a).[15b] The crystalline structure of the Zn-CCOF was determined by PXRD, FT-IR and N_2 adsorption-desorption measurements (Figure S12-S14). The result of ICP-OES measurement confirms that the average contents of Zn in Zn-CCOF is 7.18%, similar to that in Zn-S-COF. The CO_2 absorption of [Emim]BF_4(56.41 wt%)@Zn-CCOF increased to 1.32 mmol·g^{-1}, superior to the parent Zn-CCOF of 0.76 mmol·g^{-1} (Figure S15). The photocatalytic CO_2 reduction tests of [Emim]BF_4@M-COFs were carried out in gas-solid phase reaction under 300 W Xe-lamp irradiations with a 420 nm filter at room temperature without adding any photosensitizers, sacrificial agents or promoters. Before photocatalysis test, all samples were coating on a glass as supporter then vacuum dried at 120 °C for 72 h to thoroughly remove pre-adsorbed CO_2 and the residual solvents molecules (Figure S16). As a result, a series of [Emim]BF_4@M-COFs with different ILs loading amounts show apparently improved CO_2-to-CO conversion activities than the parent COFs (Figure S17). The optimal photocatalytic CO_2-to-CO conversion rates of 267.95 and 128.63 μmol·g^{-1}·h^{-1} were observed

for [Emim]BF_4(56.41 wt%)@Zn-S-COF and [Emim]BF_4(56.41 wt%)@Zn-CCOF , which are about 17 and 15 times higher than that of the pristine M-COFs, respectively (Figure 3b and S18). It was found that the optimal loading volume of ILs in [Emim]BF_4@M-COFs for the photocatalytic activity is comparable to the measured pore volumes of M-COFs, which may ensure the ILs were mainly incorporated into the pores of M-COFs and lead to a higher CO_2 absorption ability. Meanwhile, H_2 and O_2 could be detected with TCD detector and the total H_2 production amount of [Emim]BF_4@Zn-S-COF and [Emim]BF_4@Zn-CCOF were 33.46 and 18.72 $\mu mol \cdot g^{-1}$ in 5 h, respectively, giving a CO production selectivity of 97.6% and 97.2% (Figure S19). The highest apparent quantum efficiency (AQE) of 2.8% was observed at a wavelength of 420 nm for [Emim]BF_4@Zn-S-COF (Figure S20).[17] It is worth noting that the CO evolution rate of [Emim]BF_4@Zn-S-COF is above two times higher than that of [Emim]BF_4@Zn-CCOF and superior than various reported MOF and COF-based photocatalysts at similar reaction condition (Table S3).

To investigate the effect of diverse metal centers on the photocatalytic CO_2 reduction activity, different metal-based M-S-COF (M = Co and Ni) were obtained by immersing Zn-S-COFs in saturated Co^{2+} or Ni^{2+} solutions for 3 days with three-times refreshing. The ICP-OES test confirms the ratios of Zn/M are in the range of 1/24~1/25 after the exchange of

metal ions (Table S4). Photocatalytic CO_2-to-CO conversion tests confirm that single metal Zn-S-COF exhibited better performance than Co or Ni based M-S-COFs (Figure S21). To investigate the effect of different ILs on the photocatalytic activity, other three ILs including [Emim]NTf_4, [Bmim]Br and [Emim]Ac were further loaded into Zn-S-COF. The results show all these ILs could improve the catalytic performance with varying degrees and the combination of [Emim]BF_4 and Zn-S-COF is more effective for photocatalytic CO_2-to-CO conversion (Figure S22).

Photocatalytic low-concentration CO_2 reduction activity of [Emim]BF_4@M-COFs was further conducted by using 15% CO_2 (85% N_2) as gas source under simulated visible light (λ≥420 nm). As shown in Figure 3c, a CO evolution amount of 529.42 and 197.13 μmol·g^{-1} in 5 h (corresponding to 105.88 and 39.43 μmol·g^{-1}·h^{-1}, respectively) was detected for [Emim]BF_4@Zn-S-COF and [Emim]BF_4@Zn-CCOF, respectively, while only neglectable CO produced for the pristine Zn-S-COF and no product was detected for pure [Emim]BF_4. Thus, the excellent photocatalytic activity of [Emim]BF_4@Zn-S-COF under diluted CO_2 atmosphere should be attributed to the contribution of the loaded ILs by realizing the enrichment of diluted CO_2. The CO_2-to-CO selectivity of [Emim]BF_4(56.41wt%)@Zn-S-COF under diluted CO_2 atmosphere was till as high as 95% (Figure S23), indicating that the photocatalytic selectivity

of the system was not affected by CO_2 concentration.[18] Notably, the high CO_2-to-CO conversion rate of [Emim]BF_4@Zn-S-COF under diluted CO_2 atmosphere is superior than all reported photocatalysts including single-component and composite systems (Table S5), implying the effectiveness of constructing three-in-one photocatalytic system with M-COFs and ILs. In addition, [Emim]BF_4@Zn-S-COF showed stable CO production activity in 5 cycling photocatalytic measurements with diluted CO_2, which prove their stable photocatalytic performance in diluted CO_2 atmosphere (Figure 3d). The PXRD FTIR and X-ray photoelectron spectroscopy (XPS) of ILs@Zn-S-COF after photocatalytic reaction have no obvious change (Figure S24-S26), implying its stability and durability in photocatalytic process. [15b, 19]

Encouraged by the above results, natural sunlight driven photocatalytic CO_2 reduction of [Emim]BF_4@Zn-S-COF in diluted CO_2 atmosphere was further carried out to evaluate its effectiveness in the imitating real application condition (Experimental details are presented in Supplementary S3). The sample was irradiated under sunlight from 10:30 am to 15:30 pm (5 h) for consecutive 7 days/cycles (from June 22 th, 2022 to June 28 th, 2022). Encouragingly, [Emim]BF_4@Zn-S-COF showed a maximal CO production rate of 126.51 $\mu mol \cdot g^{-1}$ (average 104.26 $\mu mol \cdot g^{-1} \cdot h^{-1}$) in 5 h irradiation of natural sunlight (Figure 3e). It is note of worthy that

this is the first report of natural sunlight driven dilute CO_2 reduction without any photosensitizer or sacrificial agent, which shows promising potential towards practical application in natural condition.

To determine that the produced CO is derived from the photoreduction of introduced CO_2, the photocatalytic test with $^{13}CO_2$ as the gas source was carried out. The peak of ^{13}CO (m/z = 29) detected in the mass spectrometer confirms that the produced CO is exclusively derived from the reduction of CO_2 (Figure 3f), which is also supported by the fact that CO cannot be detected under argon atmosphere in the control experiments (Figure S27). Moreover, when $H_2{}^{18}O$ was used to replace H_2O, $^{18}O_2$ (m/z = 36) was detected in the mass spectrometer, confirming that the CO_2 reduction process is accompanied with H_2O oxidation reaction (Figure 3g).

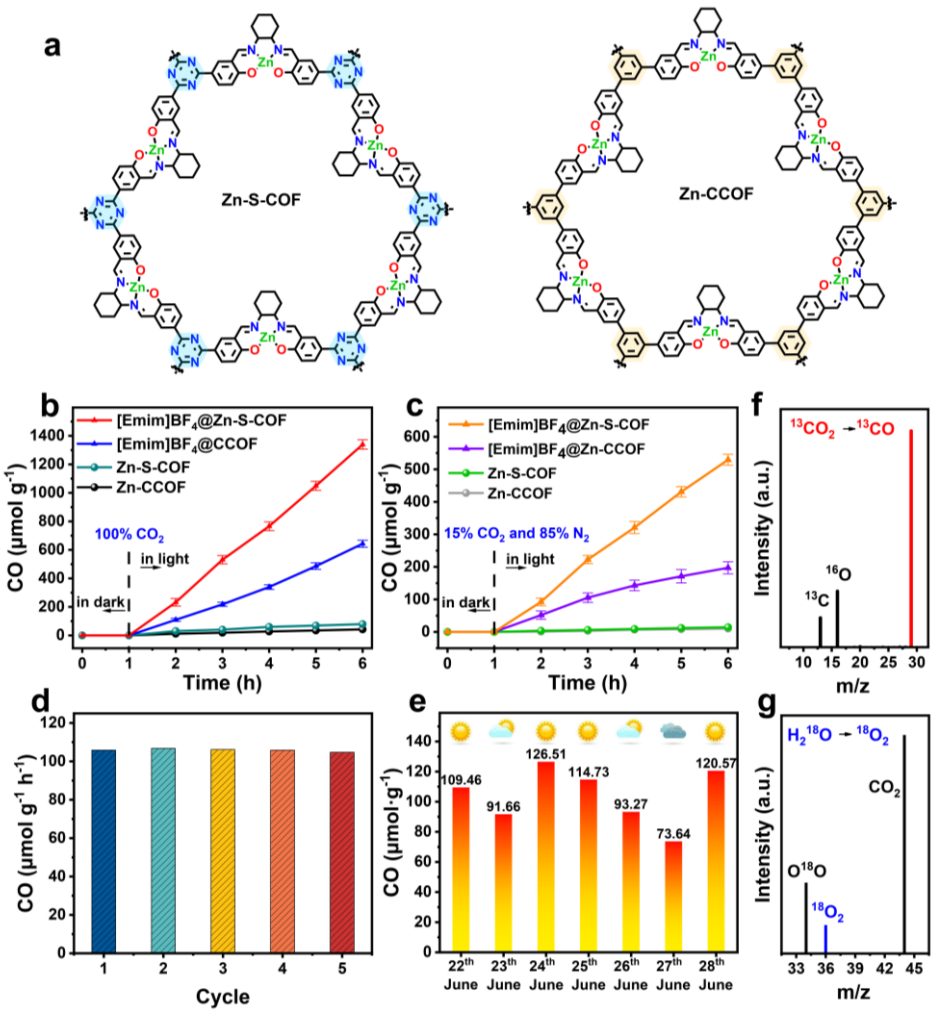

Figure 3. Structural comparison and photo-catalytic performances. (a) The structural diagram of Zn-S-COF and Zn-CCOF. (b) Time-yield plots of performance of photocatalytic gas-solid CO_2 reduction to CO. (c) Performance of photocatalytic CO_2 reduction to CO with diluted CO_2 (15% CO_2 and 85% N_2). (d) Cycling performance of [Emim]BF_4@Zn-S-COF with diluted CO_2 (15% CO_2 and 85% N_2). (e) Photocatalytic CO_2 reduction to CO driven by natural sunlight

with diluted CO_2 (15% CO_2 and 85% N_2). (f) Photocatalytic reduction of [Emim]BF_4@Zn-S-COF $^{13}CO_2$ to ^{13}CO mass spectrometry (m/z = 29). (g) Photocatalytic oxidation of [Emim]BF_4@Zn-S-COF $H_2{}^{18}O$ to $^{18}O_2$ mass spectrometry (m/z = 36).

To determine the band structure of Zn-S-COF and Zn-CCOF, the UV-vis diffuse reflection spectra (DRS) and Mott-Schottky (MS) measurements were carried out. As shown in **Figure 4**a, Zn-S-COF and Zn-CCOF show strong absorption at 380~600 nm with the calculated band gaps of 2.72 and 2.93 eV, respectively. According to MS measurements, the flat band potentials of Zn-S-COF and Zn-CCOF are -0.74 and -0.82 V vs Ag/AgCl, respectively (Figure S28 and S29). Thus, the conduction band (CB) positions of Zn-S-COF and Zn-CCOF were estimated to be -0.65 and -0.73 V (*vs*. NHE, pH = 7), respectively. Combining the band gaps and CB positions, the valence band (VB) positions of Zn-S-COF and Zn-CCOF were calculated to be 2.07 and 2.20 V, respectively. Based on the above results, it is clear that these two COFs are thermodynamic feasible for CO_2-to-CO reduction (-0.52 V *vs*. NHE, pH = 7) and simultaneous H_2O oxidation producing O_2 (0.82 V *vs*. NHE, pH = 7) (Figure 4b). [20]

The photoelectric tests for these materials were performed to explore the effects of constructing triazine rings in COFs and loading [Emim] BF_4 on the behavior of charge

carriers. The electrochemical impedance spectroscopy (EIS) measurements show the radius of the Nyquist curve of Zn-S-COF is smaller than that of Zn-CCOF, and it further reduced after loading [Emim]BF_4 (Figure S30), indicating a smaller charge transport resistance in Zn-S-COF. For the transient photocurrent responses (Figure 4c), Zn-S-COF shows stronger photocurrent intensity than that of Zn-CCOF, and the photocurrent of [Emim]BF_4@Zn-S-COF is also superior than that of [Emim]BF_4@Zn-CCOF, demonstrating a better separation ability of photogenerated charges in Zn-S-COF especially after loading ILs. As shown in Figure 4d and 4e, Zn-S-COF and [Emim]BF_4@Zn-S-COF exhibit obviously quenched photoluminescence (PL) emissions but longer PL lifetimes than that of Zn-CCOF and [Emim]BF_4@Zn-CCOF, respectively, meaning an extended lifetime of photogenerated active electrons for photocatalytic reaction.[7d] The room-temperature electron paramagnetic resonance (EPR) spectra of all photocatalysts exhibited a signal at g = 2.003 field (Figure 4f). In comparison, the intensities of EPR signals from Zn-S-COF is apparently higher than that of Zn-CCOF, which can be further enhanced after loading ILs as the EPR signals from [Emim]BF_4@Zn-S-COF is also higher than that of [Emim]BF_4@Zn-CCOF. The results of EPR measurements indicate that a stronger electron delocalization existed in the Zn-S-COF compared to Zn-CCOF photocatalyst.[21]

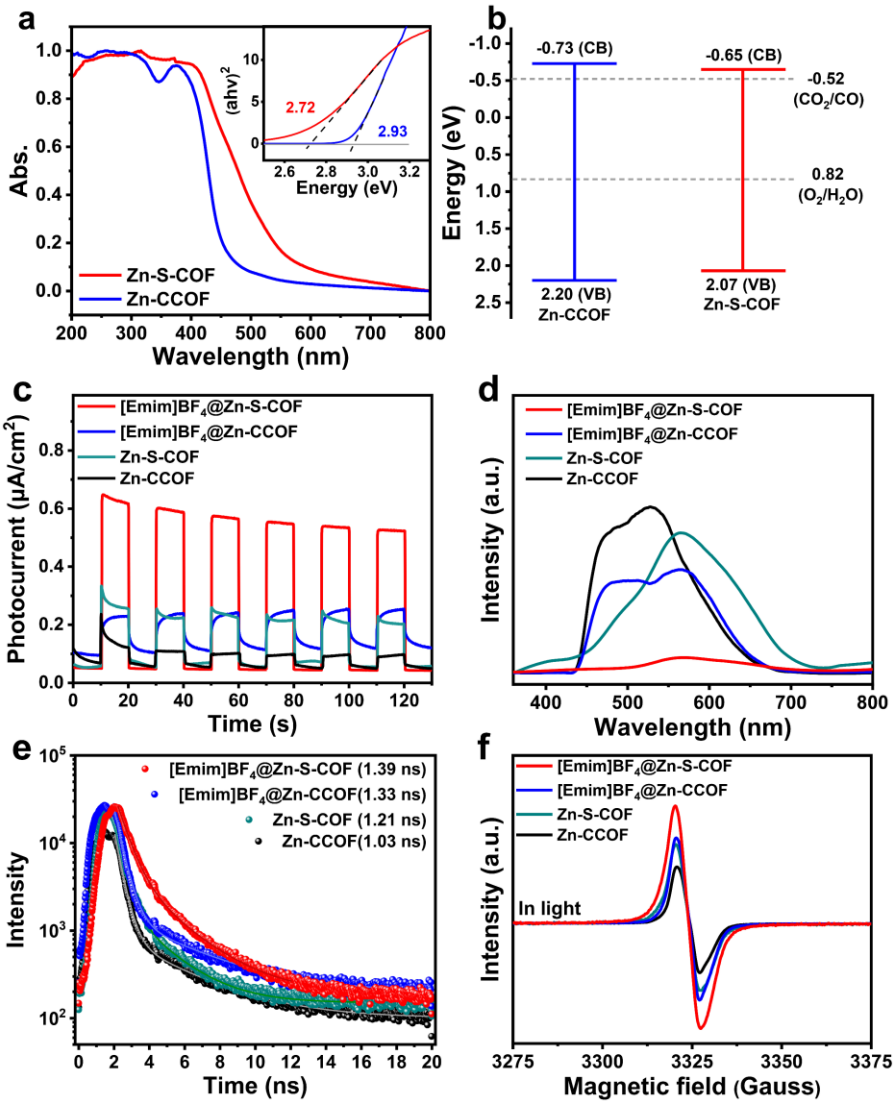

Figure 4. Characterizations of the optical properties for Zn-S-COF, Zn-CCOF, [Emim]BF_4@Zn-S-COF and [Emim]BF_4@Zn-CCOF. a) UV-vis absorption spectra of Zn-S-COF and Zn-CCOF (Inset: optical bandgap). (b) Schematic diagram of energy band

structure. (c) Transient photocurrent responses. (d) Photoluminescence spectra. (e) Time-resolved PL spectra. (f) EPR spectra with 420 nm light irradiation.

To elucidate the stability of Zn-Salen units of Zn-S-COF in photocatalytic reaction, X-ray absorption spectroscopy (XAS) was performed for Zn-S-COF after photocatalytic reaction and removing [Emim]BF_4. The Zn K-edge X-ray absorption near-edge structure (XANES) is shown in **Figure 5**a. The position of Zn K-edge is between Zn Foil and ZnO, and closer to ZnPc, which implies that the Zn in Zn-S-COF has more positive charges than Zn foil and fewer positive charges than ZnO, between 0 and +2 positive valence state.[22] As presented in Figure 5b, the Fourier transform (FT) EXAFS spectra of the Zn K-edge for Zn-S-COF appeared a main peak at 1.49 Å, which located on the scattering paths of Zn-N in ZnPc and Zn-O bonds in ZnO, indicating that Zn in Zn-S-COF was coordinated by both N and O atoms (Table S6). The coordination number and coordination structure of the Zn center in Zn-S-COF were determined by the EXAFS fitting results of the first shell, which proved that the Zn atom in Zn-S-COF is coordinated by two N and two O atoms (Figure 5c). Combined with the fitting results of the K space of Zn-S-COF (Figure 5d), it can be further inferred that Zn exhibits Zn-N_2O_2 coordination configuration with the average bond length of 2.03 and 1.94 Å for Zn-O and Zn-N, respectively (Table S6 and Figure S31).[23] The wavelet transforms

(WT) contours show that the maxima in ZnO and ZnPc are 5.05, 7.42 and 5.75 $Å^{-1}$, respectively, and these peaks correspond to Zn-O, Zn-Zn and Zn-N bonds, respectively (Figure 5e). For the WT of Zn-S-COF, the maximum intensity appeared at 4.84 $Å^{-1}$, which is attributed to the Zn-O bond and Zn-N.[24] Since the bond lengths of Zn-O and Zn-N are close, the WT appears as a single peak. All the above analyses clearly indicate the stable Zn-N_2O_2 coordination mode of Zn ions in the Salen unit of Zn-S-COF.

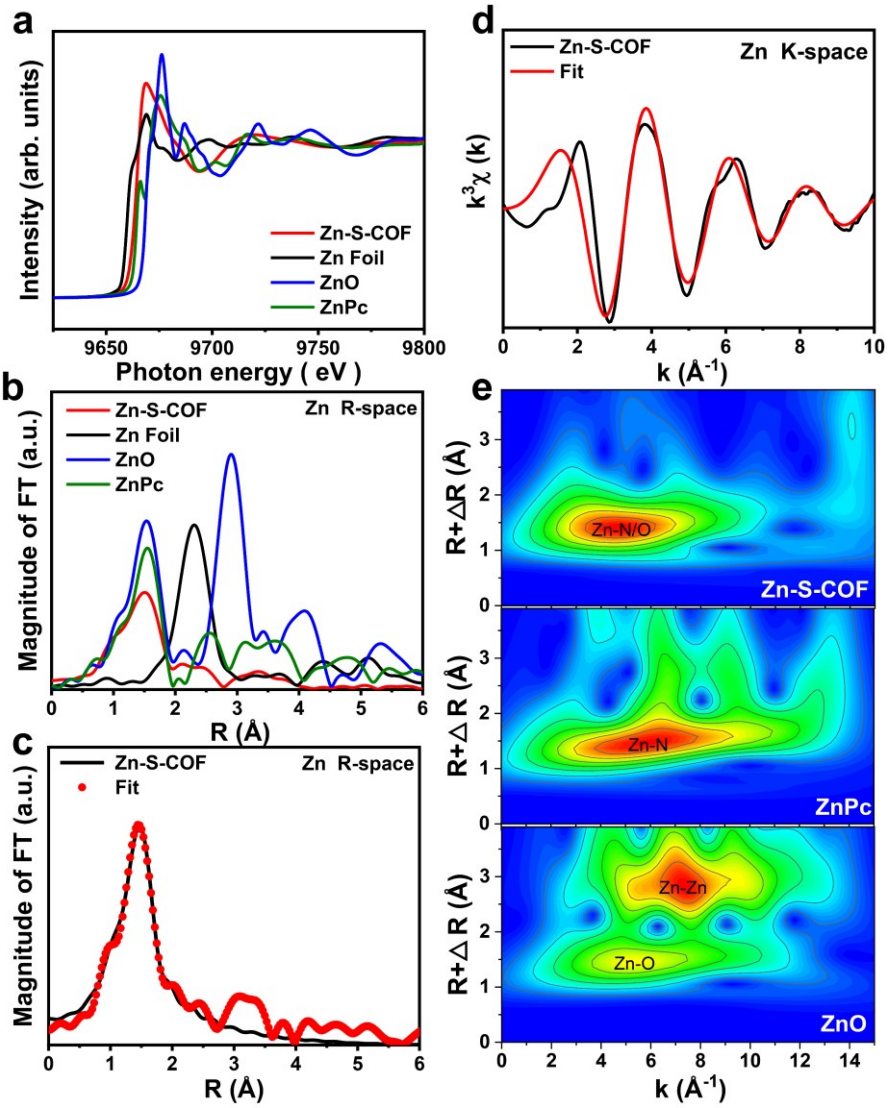

Figure 5. X-ray absorption spectroscopy analysis. (a) XANES spectra of Zn-S-COF, Zn Foil, ZnO and ZnPc, (b) FT-EXAFS spectra of Zn-S-COF, Zn Foil, ZnO and ZnPc, (c) EXAFS fitting results of Zn-S-COF at R-space, (d) EXAFS fitting results of Zn-S-COF at K-space, (e) Wavelet transform of Zn-S-COF, ZnPc and ZnO.

The in situ diffuse reflectance infrared Fourier transform spectra (DRIFTS) measurement was carried out for [Emim]BF_4@Zn-S-COF to detect the reaction intermediates in the photocatalytic CO_2 reduction process. As shwon in **Figure 6**a and 6b, the characteristic peaks at 2331 and 2362 cm^{-1} were observed obviously after the introduction of CO_2, which are attributed to the stretching vibration of the CO_2 molecules adsorbed on the surface of the photocatalyst.[25] In addition, several carboxylate complexes and activated CO_2 intermediates were detected: the peak at 1268 cm^{-1} coresponds to the bidentate carbonate (b-CO_3^{2-});[26] the peaks at 1335 and 1492 cm^{-1} are ascribed to the monodentate carbonate (m-CO_3^{2-});[27] the bands at 1378 and 1430 cm^{-1} are assigned to the bicarbonate radical (HCO_3^-);[28] the peaks at 1240 and 1689 cm^{-1} were attributed to the characteristic peaks of stretching vibration of $\cdot CO_2^-$.[29] All the detected carboxylate complexes species are reaction intermediates for CO_2-to-CO production. In addition, the characteristic peaks around 1574~1638 cm^{-1} can be assigned to *COOH, which is an important reaction intermediate of CO production and also reveals the important transformation process of CO_2 in the photocatalytic reaction.[30] The absorption peaks of all the detected intermediates become stronger gradually with the prolonging of irradiation time, which implies the progress of the photocatalytic reaction.

Density functional theory (DFT) calculations were performed to explore photocatalytic reaction mechanism (Calculation details see Supplementary S4) by using the simplified structural model (Figure S32). The CO_2-to-CO reaction processes of Zn-S-COF and Zn-CCOF were compared to further clarify the contribution of triazine core. Although the CO_2 adsorption and the protonation process of *COOH is similar in Zn-S-COF and Zn-CCOF, there is a major difference in CO desorption process from the reactive sites. The generated CO molecules tend to more easily desorb on Zn-S-COF in comparison with Zn-CCOF, which leads to a high CO yield (Figure 6c). Thus, the possible mechanism for artificial photosynthesis of CO_2 reduction on Zn-S-COF was reasonably proposed (Figure S33).

The diversity of water oxidation process of these two M-COFs in artificial photosynthetic reaction was further investigated. The calculated UV-vis absorption spectra of Zn-S-COF (Figure S34a) is great agreement with the experiment results. Thus, from the corresponding orbital transitions and the distribution of electron and hole for each excited state (Figure S34b and c), it can be clearly convinced that the photo-excited hole was concentrated on the benzene ring, and the C atoms in the benzene ring can serve as H_2O oxidation active sites.[31] Although all the sp^2 -hybridized C were the potential H_2O oxidation active sites of Zn-S-COF, the C1, C4 and C6 were excluded since the high steric hindrance leading to structural

distortion in the first step of the *OH formation. Thus the possible H_2O oxidation active sites should be concentrated on the C2, C3 and C5 atoms. According to previous work,[32] two possible mechanisms, single-site and dual-site mechanisms of the H_2O oxidation reaction, were considered in calculation (Figure 6e and S35). The results demonstrate that the free energy barrier of the rate-determining step for single-site process was obviously higher than that for dual-site process (Figure S36). Thus, the dual-site paths of C2 site (C2D) were considered as the most reactive path in view of its thermodynamically more favorable than others. Compared to the ΔG for each step in C2D paths of Zn-S-COF and Zn-CCOF (Figure 6d), Zn-S-COF shows a lower ΔG for the formation of OH*, O*OH*, and OO* intermediates, confirming the effectiveness of constructing triazine rings in Zn-S-COF in promoting H_2O oxidation activity.

To explore the probable role of $[Emim]BF_4$ in photocatalytic CO_2 reduction process, further calculation was performed for $[Emim]BF_4$@Zn-S-COF. The results indicate that the CO_2 molecules tend to spontaneously combining with $Emim^+$ to form Emim-CO_2 with the ΔG of -3.88 eV (Figure S37), indicating the excellent ability of $[Emim]BF_4$ to capture diluted CO_2. The ΔG of the adsorption of CO_2 molecules and formation of *COOH were significantly reduced for the contribution of $[Emim]BF_4$. The photocatalytic CO_2 reduction process of

[Emim]BF_4@Zn-S-COF was shown in Figure 6e. The $Emim^+$ firstly capture low-concentration CO_2 and create an enriched CO_2 atmosphere, then transfer the CO_2 to Zn active sites of the Zn-S-COF. Subsequently, $Emim^+$ provides a proton-electron pair to facilitate hydrogenation processes (*COOH-Emim formation). The *COOH-Emim intermediate further get a photogenerated electron from COF backbone and a proton, forming the resultant CO product. All the calculation results support that ILs really plays an important role in facilitating artificial photosynthesis of low-concentration CO_2.

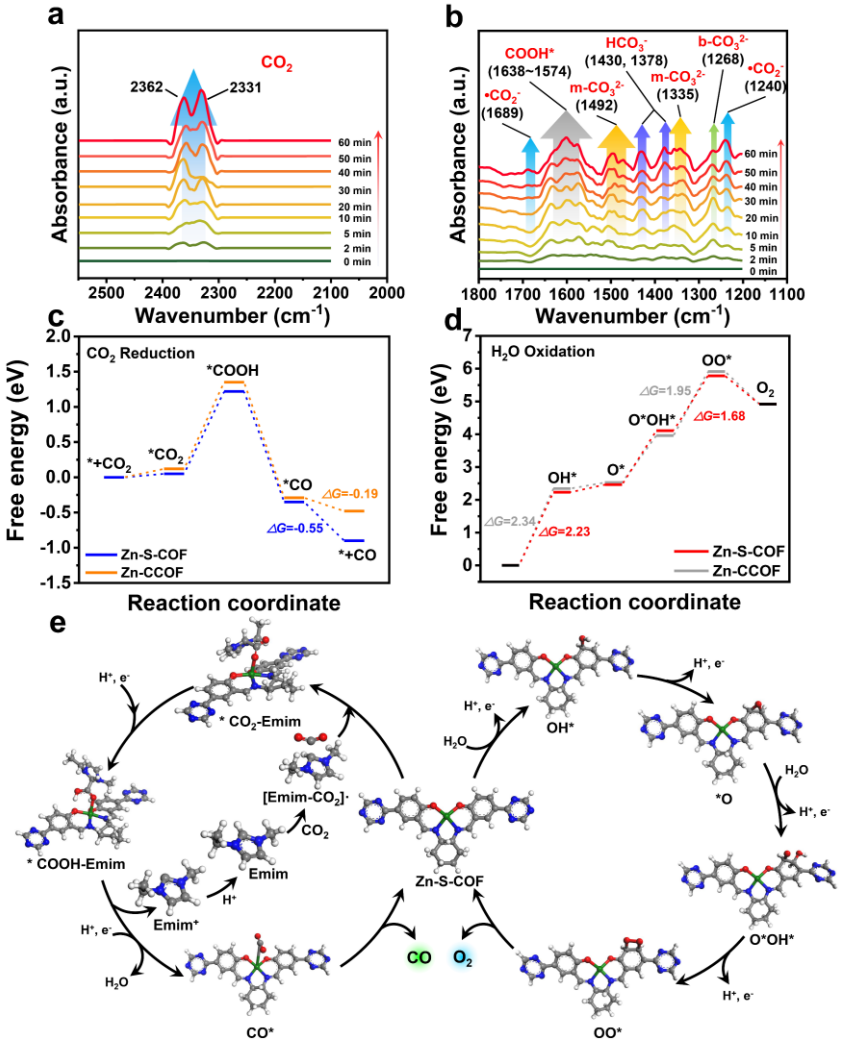

Figure 6. DFT calculations and the proposed artificial photosynthesis mechanism. (a) In situ DRIFTS of [Emim]BF_4@Zn-S-COF for CO_2 adsorption. (b) In situ DRIFTS of [Emim]BF_4@Zn-S-COF for CO_2 reduction in the dark (background) and under visible light irradiation (Irradiation time 2, 5, 10, 20, 30, 40, 50, 60 min, respectively). (c) Free energy

profile of Zn-S-COF and Zn-CCOF in the CO_2 reduction process. (d) Free energy profile of Zn-S-COF and Zn-CCOF in the H_2O oxidation process. (e) Schematic diagram of proposed artificial photosynthesis mechanism for [Emim]BF_4@Zn-S-COF.

3. Conclusion

In summary, a three-in-one artificial photosynthetic system with CO_2 reduction, H_2O oxidation and CO_2 enrichment sites was developed based on M-COFs and ILs for diluted CO_2 reduction. A triazine core-based Zn-S-COF with designed CO_2 reduction and H_2O oxidation sites was synthesized to serve as the host of photocatalysts, then ILs acting as CO_2 enrichment component was further introduced into the pores of Zn-S-COF. An ultrahigh visible-light-driven CO_2-to-CO conversion rate of 267.95 $\mu mol \cdot g^{-1} \cdot h^{-1}$ was observed for [Emim]BF_4@Zn-S-COF. Under diluted CO_2 (15%) atmosphere, the CO evolution rate was as high as 105.88 $\mu mol \cdot g^{-1} \cdot h^{-1}$, and natural sunlight driven diluted CO_2 reduction rate also reached 126.51 $\mu mol \cdot g^{-1}$ in 5 h. The results of experiments and theoretical calculation imply that the loaded [Emim]BF_4 forms an enriched CO_2 atmosphere, and the triazine ring in Zn-S-COF promotes the activity of H_2O oxidation and CO_2 reduction sites in photocatalytic diluted CO_2 reduction reaction. This work provides a new and promising strategy towards the

practical application of solar photocatalysis for directly enriching and converting diluted CO_2 to fuels with industrial exhaust gas.

Conflict of Interest

The authors declare of no conflict of interest.

Supporting Information

Supporting Information is available from the Wiley Online Library or from the author.

Acknowledgements

This work is financially supported by the National Natural Science Foundation of China (No. 22178077), Shandong Provincial Natural Science Foundation (No. ZR2022MB126), and the Postdoctoral Scientific Research Start-up Project in Heilongjiang Province (No. LBH-Q19111), Open Fund of Key Laboratory for Advanced Technology in Environmental Protection of Jiangsu Province (JBGS013).

Received: ((will be filled in by the editorial staff))

Revised: ((will be filled in by the editorial staff))

Published online: ((will be filled in by the editorial staff))

References

[1] a)C. Gao, J. Low, R. Long, T. Kong, J. Zhu, Y. Xiong, *Chem. Rev.* **2020**, 120, 12175; b)Y. A. Wu, I. McNulty, C. Liu, K. C. Lau, Q. Liu, A. P. Paulikas, C. J. Sun, Z. H. Cai, J. R. Guest, Y. Ren, V. Stamenkovic, L. A. Curtiss, Y. Z. Liu, T. Rajh, *Nat. Energy* **2019**, 4, 957; c)W. H. Zhang, A. R. Mohamed, W. J. Ong, *Angew. Chem. Int. Ed.* **2020**, 59, 22894; d)T. T. Kong, Y. W. Jiang, Y. J. Xiong, *Chem. Soc. Rev.* **2020**, 49, 6579.

[2] a)L. M. Wang, W. L. Chen, D. D. Zhang, Y. P. Du, R. Amal, S. Z. Qiao, J. W. Bf, Z. Y. Yin, *Chem. Soc. Rev.* **2019**, 48, 5310; b)H. Shirley, X. J. Su, H. Sanjanwala, K. Talukdar, J. W. Jurss, J. H. Delcamp, *J. Am. Chem. Soc.* **2019**, 141, 6617; c)J. W. Wang, L. Jiang, H. H. Huang, Z. J. Han, G. F. Ouyang, *Nat. Commun.* **2021**, 12, 4276 4276.

[3] a)M. Xiao, Z. L. Wang, M. Q. Lyu, B. Luo, S. C. Wang, G. Liu, H. M. Cheng, L. Z. Wang, *Adv. Mater.* **2019**, 31, 1801369, 1801369; b)C. Hu, S. C. Tu, N. Tian, T. Y. Ma, Y. H. Zhang, H. W. Huang, *Angew. Chem. Int. Ed.* **2021**, 60, 16309.

[4] a)H. Kumagai, Y. Tamaki, O. Ishitani, *Acc. Chem. Res.* **2022**, 55, 978; b)E. Pugliese, P. Gotico, I. Wehrung, B. Boitrel, A. Quaranta, M.-H. Ha-Thi, T. Pino, M. Sircoglou, W. Leibl, Z. Halime, A. Aukauloo, *Angew. Chem. Int. Ed.* **2022**, 61, 202117530; c)Y. Feng, C. Wang, P. Cui, C. Li, B. Zhang, L. Gan, S. Zhang, X. Zhang, X. Zhou, Z. Sun, K. Wang, Y. Duan, H. Li, K. Zhou, H. Huang, A. Li, C. Zhuang, L. Wang, Z. Zhang, X. Han, *Adv. Mater.* **2022**, 2109074, 2109074.

[5] a)L. Ran, Z. Li, B. Ran, J. Cao, Y. Zhao, T. Shao, Y. Song, M. K. H. Leung, L. Sun, J. Hou, *J. Am. Chem. Soc.* **2022**, 144, 17097; b)Z. Zhao, D. Zheng, M. Guo, J. Yu, S. Zhang, Z. Zhang, Y. Chen, *Angew. Chem. Int. Ed.* **2022**, 61, e202200261; c)H. Wang, Z. T. Zeng, P. Xu, L. S. Li, G. M. Zeng, R. Xiao, Z. Y. Tang, D. L. Huang, L. Tang, C. Lai, D. N. Jiang, Y. Liu, H. Yi, L. Qin, S. J. Ye, X. Y. Ren, W. W. Tang, *Chem. Soc. Rev.* **2019**, 48, 488; d)Y. H. Liu, L. M. Liu, X. Chen, Y. Liu, Y. Han, Y. Cui, *J. Am. Chem. Soc.* **2021**, 143, 3509.

[6] a)W. B. Liu, X. K. Li, C. M. Wang, H. H. Pan, W. P. Liu, K. Wang, Q. D. Zeng, R. M. Wang, J. Z. Jiang, *J. Am. Chem. Soc.* **2019**, 141, 17431; b)C.-J. Wu, X.-Y. Li, T.-R. Li, M.-Z. Shao, L.-J. Niu, X.-F. Lu, J.-L. Kan, Y. Geng, Y.-B. Dong, *J. Am. Chem. Soc.* **2022**; c)J. Li, X. C. Jing, Q. Q. Li, S. W. Li, X. Gao, X. Feng, B. Wang, *Chem. Soc. Rev.* **2020**, 49, 3565; d)B. Han, X. Ding, B. Q. Yu, H. Wu, W. Zhou, W. P. Liu, C. Y. Wei, B. T. Chen, D. D. Qi, H. L. Wang, K. Wang, Y. L. Chen, B. L. Chen, J. Z. Jiang, *J. Am. Chem. Soc.* **2021**, 143, 7104.

[7] a)Y. M. Li, L. Yang, H. J. He, L. Sun, H. L. Wang, X. Fang, Y. L. Zhao, D. Y. Zheng, Y. Qi, Z. Li, W. Q. Deng, *Nat. Commun.* **2022**, 13, 1355; b)H. Dong, M. Lu, Y. Wang, H.-L. Tang, D. Wu, X. Sun, F.-M. Zhang, *Appl. Catal. B* **2022**, 303, 120897, 120897; c)S. Yang, R. Sa, H. Zhong, H. Lv, D. Yuan, R. Wang, *Adv. Funct. Mater.* **2022**, 2110694, 2110694; d)Y. N. Gong, W. H. Zhong, Y. Li, Y. Z. Qiu, L. R. Zheng, J. Jiang, H. L. Jiang, *J. Am. Chem. Soc.* **2020**, 142, 16723.

[8] a)Z. J. Mu, Y. H. Zhu, B. X. Li, A. W. Dong, B. Wang, X. Feng, *J. Am. Chem. Soc.* **2022**, 144, 5145; b)C. Y. Xing, P. Mei, Z. J. Mu, B. X. Li, X. Feng, Y. Y. Zhang, B. Wang, *Angew. Chem. Int. Ed.* **2022**, 202201378; c)S. D. Diwakara, W. S. Y. Ong, Y. H. Wijesundara, R. L. Gearhart, F. C. Herbert, S. G. Fisher, G. T. McCandless, S. B.

Alahakoon, J. J. Gassensmith, S. C. Dodani, R. A. Smaldone, *J. Am. Chem. Soc.* **2022**, 144, 2468.

[9] a)Y. R. Wang, H. M. Ding, S. N. Sun, J. w. Shi, Y. L. Yang, Q. Li, Y. F. Chen, S. L. Li, Y. Q. Lan, *Angew. Chem. Int. Ed.* **2022**, 61, e202212162; b)H. J. Yu, J. Y. Li, Y. H. Zhang, S. Q. Yang, K. L. Han, F. Dong, T. Y. Ma, H. W. Huang, *Angew. Chem. Int. Ed.* **2019**, 58, 3880.

[10] a)W. Ying, J. S. Cai, K. Zhou, D. K. Chen, Y. L. Ying, Y. Guo, X. Q. Kong, Z. P. Xu, X. S. Peng, *ACS Nano* **2018**, 12, 5385; b)S. Supasitmongkol, P. Styring, *Energy Environ. Sci.* **2010**, 3, 1961; c)F. F. Chen, K. Huang, Y. Zhou, Z. Q. Tian, X. Zhu, D. J. Tao, D. Jiang, S. Dai, *Angew. Chem. Int. Ed.* **2016**, 55, 7166.

[11] a)O. Nordness, J. F. Brennecke, *Chem. Rev.* **2020**, 120, 12873; b)B. S. Wang, L. Qin, T. C. Mu, Z. M. Xue, G. H. Gao, *Chem. Rev.* **2017**, 117, 7113; c)G. K. Cui, J. J. Wang, S. J. Zhang, *Chem. Soc. Rev.* **2016**, 45, 4307; d)S. J. Yu, P. K. Jain, *Nat. Commun.* **2019**, 10, 2020, 2022; e)M. Armand, F. Endres, D. R. MacFarlane, H. Ohno, B. Scrosati, *Nat. Mater.* **2009**, 8, 621.

[12] a)W. F. Jiang, X. S. Li, G. Gao, F. Wu, C. Luo, L. Q. Zhang, *Chem. Eng. J.* **2022**, 445, 136767; b)Q. R. Sheridan, W. F. Schneider, E. J. Maginn, *Chem. Rev.* **2018**, 118, 5242; c)Q. Sun, Y. Zhao, W. Ren, C. Zhao, *Appl. Catal. B* **2022**, 304, 120963.

[13] a)J. Avila, L. F. Lepre, C. C. Santini, M. Tiano, S. Denis Quanquin, K. Chung Szeto, A. A. H. Padua, M. Costa Gomes, *Angew. Chem. Int. Ed.* **2021**, 60, 12876; b)M. Zeeshan, V. Nozari, M. B. Yagci, T. Isik, U. Unal, V. Ortalan, S. Keskin, A. Uzun, *J. Am. Chem. Soc.* **2018**, 140, 10113.

[14] a)H. Li, J. H. Ding, X. Y. Guan, F. Q. Chen, C. Y. Li, L. K. Zhu, M. Xue, D. Q. Yuan, V. Valtchev, Y. S. Yan, S. L. Qiu, Q. R. Fang, *J. Am. Chem. Soc.* **2020**, 142, 13334; b)S. Wang, Q. Sun, W. Chen, Y. Q. Tang, B. Aguila, Y. X. Pan, A. Zheng, Z. Y. Yang, L. Wojtas, S. Ma, F. S. Xiao, *Matter* **2020**, 2, 416.

[15] a)R. Chen, Y. Wang, Y. Ma, A. Mal, X.-Y. Gao, L. Gao, L. Qiao, X.-B. Li, L.-Z. Wu, C. Wang, *Nat. Commun.* **2021**, 12, 1354; b)X. Han, Q. C. Xia, J. J. Huang, Y. Liu, C. X. Tan, Y. Cui, *J. Am. Chem. Soc.* **2017**, 139, 8693; c)V. S. Vyas, F. Haase, L. Stegbauer, G. Savasci, F. Podjaski, C. Ochsenfeld, B. V. Lotsch, *Nat. Commun.* **2015**, 6, 8508.

[16] W. J. Xue, Z. J. Li, H. L. Huang, Q. Y. Yang, D. H. Liu, Q. Xu, C. L. Zhong, *Chem. Eng. Sci.* **2016**, 140, 1.

[17] Y.-N. Gong, X. Guan, H.-L. Jiang, *Coord. Chem. Rev.* **2023**, 475, 214889.

[18] a)J. Ding, X. Guan, J. Lv, X. Chen, Y. Zhang, H. Li, D. Zhang, S. Qiu, H.-L. Jiang, Q. Fang, *J. Am. Chem. Soc.* **2023**, 145, 3248; b)Y. Qian, D. Li, Y. Han, H.-L. Jiang, *J. Am. Chem. Soc.* **2020**, 142, 20763.

[19] M. Lu, M. Zhang, C. G. Liu, J. Liu, L. J. Shang, M. Wang, J. N. Chang, S. L. Li, Y. Q. Lan, *Angew. Chem. Int. Ed.* **2021**, 60, 4864.

[20] a)P. J. Yang, R. R. Wang, H. L. Tao, Y. F. Zhang, M. M. Titirici, X. C. Wang, *Appl. Catal. B* **2021**, 280, 119454, 119454; b)H. R. Park, A. U. Pawar, U. Pal, T. R. Zhang, Y. S. Kang, *Nano Energy* **2021**, 79, 105483 105483.

[21] B. G. Wu, L. P. Zhang, B. J. Jiang, Q. Li, C. G. Tian, Y. Xie, W. Z. Li, H. G. Fu, *Angew. Chem., Int. Ed.* **2021**, 60, 4815.

[22] a)Y. L. Jia, Z. Q. Xue, J. Yang, Q. L. Liu, J. H. Xian, Y. C. Zhong, Y. M. Sun, X. X. Zhang, Q. H. Liu, D. X. Yao, G. Q. Li, *Angew. Chem. Int. Ed.* **2022**, 61, 202110838, e202110838;

b)X. Y. Dong, Y. N. Si, Q. Y. Wang, S. Wang, S. Q. Zang, *Adv. Mater.* **2021**, 33, 2101568.

[23] a)Y. Guo, Y. C. Wang, Y. Shen, Z. Y. Cai, Z. Li, J. Liu, J. W. Chen, C. Xiao, H. C. Liu, W. B. Lin, C. Wang, *J. Am. Chem. Soc.* **2020**, 142, 21493; b)L. J. Zhang, W. W. Cai, N. Z. Bao, *Adv. Mater.* **2021**, 33, 2100745, 2100745.

[24] a)C. Negri, T. Selleri, E. Borfecchia, A. Martini, K. A. Lomachenko, T. V. W. Janssens, M. Cutini, S. Bordiga, G. Berlier, *J. Am. Chem. Soc.* **2020**, 142, 15884; b)W. Zhang, C. Huang, Q. Xiao, L. Yu, L. Shuai, P. An, J. Zhang, M. Qiu, Z. Ren, Y. Yu, *J. Am. Chem. Soc.* **2020**, 142, 11417.

[25] a)M. Wang, M. Shen, X. X. Jin, J. J. Tian, M. L. Li, Y. J. Zhou, L. X. Zhang, Y. S. Li, J. L. Shi, *ACS Catal.* **2019**, 9, 4573; b)X. L. Yang, S. Y. Wang, N. Yang, W. Zhou, P. Wang, K. Jiang, S. Li, H. Song, X. Ding, H. Chen, J. H. Ye, *Appl. Catal. B* **2019**, 259, 118088, 118088.

[26] J. Wu, X. D. Li, W. Shi, P. Q. Ling, Y. F. Sun, X. C. Jiao, S. Gao, L. Liang, J. Q. Xu, W. S. Yan, C. M. Wang, Y. Xie, *Angew. Chem. Int. Ed.* **2018**, 57, 8719.

[27] N. X. Li, B. B. Wang, Y. Y. Si, F. Xue, J. C. Zhou, Y. J. Lu, M. C. Liu, *ACS Catal.* **2019**, 9, 5590.

[28] a)X. D. Li, Y. F. Sun, J. Q. Xu, Y. J. Shao, J. Wu, X. L. Xu, Y. Pan, H. X. Ju, J. F. Zhu, Y. Xie, *Nat. Energy* **2019**, 4, 690; b)Y. M. Liu, S. Chen, X. Quan, H. T. Yu, *J. Am. Chem. Soc.* **2015**, 137, 11631.

[29] J. P. Sheng, Y. He, J. Y. Li, C. W. Yuan, H. W. Huang, S. Y. Wang, Y. J. Sun, Z. M. Wang, F. Dong, *ACS Nano* **2020**, 14, 13103.

[30] S. Karmakar, S. Barman, F. A. Rahimi, T. K. Maji, *Energy Environ. Sci.* **2021**, 14, 2429.

[31] a)C. H. Yang, Z. D. Yang, R. Zhang, G. L. Zhang, *Chem. Phys.* **2019**, 517, 104; b)C. H. Yang, Z. D. Yang, H. Dong, N. Sun, Y. Lu, F. M. Zhang, G. L. Zhang, *ACS Energy Lett.* **2019**, 4, 2251.

[32] a)Y. Yang, X. Y. Chu, H. Y. Zhang, R. Zhang, Y. H. Liu, F. M. Zhang, M. Lu, Z. D. Yang, Y. Q. Lan, *Nat. Commun.* **2023**, 14, 593; b)Y. Y. Wan, L. Wang, H. X. Xu, X. J. Wu, J. L. Yang, *J. Am. Chem. Soc.* **2020**, 142, 4508.

A three-in-one photocatalytic system of CO_2 enrichment, CO_2 reduction and H_2O oxidation sites were designed for diluted CO_2 reduction, and the [Emim]BF_4@Zn-Salen-COF show excellent visible-light-driven and natural-sunlight-driven CO_2-to-CO conversion activity under diluted CO_2 (15%) atmosphere.

Yan Yang[a,c,†], Hong-Yu Zhang[a,c,†], Ya Wang[a,†], Lu-Hua Shao[a], Liang Fang[a], Hong Dong[a], Meng Lu[b], Long-Zhang Dong[b], Ya-Qian Lan[b] and Feng-Ming Zhang[a,]*

Integrating Enrichment, Reduction and Oxidation Sites in One System for Artificial Photosynthetic diluted CO_2 Reduction